REGULAR ARTICLE

blood advances

Altered enhancer-promoter interaction leads to *MNX1* expression in pediatric acute myeloid leukemia with t(7;12)(q36;p13)

Dieter Weichenhan,[1,*] Anna Riedel,[1,*] Etienne Sollier,[1,*] Umut H. Toprak,[2,*] Joschka Hey,[1] Kersten Breuer,[1] Justyna A. Wierzbinska,[1] Aurore Touzart,[1] Pavlo Lutsik,[1] Marion Bähr,[1] Anders Östlund,[3] Tina Nilsson,[4] Susanna Jacobsson,[4] Marcel Edler,[4] Ahmed Waraky,[3,4] Yvonne Lisa Behrens,[5] Gudrun Göhring,[5] Brigitte Schlegelberger,[5] Clemens Steinek,[6] Hartmann Harz,[6] Heinrich Leonhardt,[6] Anna Dolnik,[7] Dirk Reinhardt,[8] Lars Bullinger,[7] Lars Palmqvist,[3,4] Daniel B. Lipka,[9-11,†] and Christoph Plass[1,10,†]

[1]Division of Cancer Epigenomics and [2]Division of Neuroblastoma Genomics, German Cancer Research Center, Heidelberg, Germany; [3]Department of Laboratory Medicine, University of Gothenburg, Gothenburg, Sweden; [4]Department of Clinical Chemistry, Sahlgrenska University Hospital, Gothenburg, Sweden; [5]Department of Human Genetics, Hannover Medical School, Hannover, Germany; [6]Faculty of Biology, Ludwig-Maximilians-Universität in Munich, Planegg-Martinsried, Germany; [7]Department of Hematology, Oncology, and Tumor Immunology, Charité-Universitätsmedizin Berlin, Corporate Member of Freie Universität Berlin and Humboldt-University Berlin, Berlin, Germany; [8]Department of Pediatric Oncology, University of Duisburg-Essen, Essen, Germany; [9]Section of Translational Cancer Epigenomics, Division of Translational Medical Oncology, German Cancer Research Center, Heidelberg, Germany; [10]German Cancer Consortium, Heidelberg, Germany; and [11]National Center for Tumor Diseases, NCT Heidelberg, a partnership between DKFZ and Heidelberg University Hospital, Heidelberg, Germany

Key Points

- Expression analysis of >1500 pediatric AML samples demonstrates *MNX1* expression as a universal feature of t(7;12)(q36;p13) AML.
- *MNX1* is activated by an enhancer-hijacking event in t(7;12)(q36;p13) AML and not, as previously postulated, by an *MNX1*::*ETV6* oncofusion.

Acute myeloid leukemia (AML) with the t(7;12)(q36;p13) translocation occurs only in very young children and has a poor clinical outcome. The expected oncofusion between break point partners (*motor neuron and pancreas homeobox 1* [*MNX1*] and *ETS variant transcription factor 6* [*ETV6*]) has only been reported in a subset of cases. However, a universal feature is the strong transcript and protein expression of MNX1, a homeobox transcription factor that is normally not expressed in hematopoietic cells. Here, we map the translocation break points on chromosomes 7 and 12 in affected patients to a region proximal to *MNX1* and either introns 1 or 2 of *ETV6*. The frequency of *MNX1* overexpression in pediatric AML is 2.4% and occurs predominantly in t(7;12)(q36;p13) AML. Chromatin interaction assays in a t(7;12)(q36;p13) induced pluripotent stem cell line model unravel an enhancer-hijacking event that explains *MNX1* overexpression in hematopoietic cells. Our data suggest that enhancer hijacking may be a more widespread consequence of translocations in which no oncofusion product was identified, including t(1;3) or t(4;12) AML.

Introduction

Acute myeloid leukemia (AML) has been successfully investigated in the past using cytogenetic analysis. This led to the discovery of numerous recurrent chromosomal translocations (eg, t(8;21)(q22; q22) or t(15;17)(q22;q12)) generating oncofusion proteins (eg, RUNX1::RUNX1T1 or PML::RARA, respectively) that drive leukemogenesis. For many years, these translocations have served as diagnostic and prognostic

Submitted 13 November 2023; accepted 27 July 2024; prepublished online on *Blood Advances* First Edition 9 August 2024. https://doi.org/10.1182/bloodadvances.2023012161.

*D.W., A.R., E.S., and U.H.T. are joint first authors.

†D.B.L. and C.P. are joint senior authors.

All cell line sequencing data generated here are based on human reference GRCh37/hg19 and were deposited in the National Center for Biotechnology Information Gene Expression Omnibus database under accession GSE244379. The patient data were deposited in the European Genome-Phenome Archive (accession number EGAS50000000130).

The full-text version of this article contains a data supplement.

markers and affected patients can now be treated with specific targeted therapies (eg, retinoic acid and arsenic trioxide in t(15;17) cases).[1] In 1998, 2 publications reported the translocation t(7;12)(q36;p13) in AML of infants[2,3] occurring predominantly in children aged <18 months and not in adult AML. A recent meta-analysis of the Nordic Society for Pediatric Hematology and Oncology (NOPHO-AML) determined that t(7;12)(q36;p13) AML constituted 4.3% of all children with AML aged <2 years and found a 3-year event-free survival of 24% (literature-based data) and 43% (NOPHO-AML data).[4] Cytogenetically, t(7;12)(q36;p13) AML is often associated with the occurrence of trisomy 19,[4,5] but no other recurrent aberrations have been described.

Reported break points in t(7;12)(q36;p13) AML have mainly been evaluated by fluorescent in situ hybridization analysis. The breakpoints on chromosome 12 (chr12) are located within intron 1 or 2 of *ETS variant transcription factor 6* (*ETV6*) and proximal to *motor neuron and pancreas homeobox 1* (*MNX1*) and within the 3' end of *nucleolar protein with MIF4G domain 1* (*NOM1*) on chr7.[6] A *MNX1*::*ETV6* fusion transcript was described only in a subset of t(7;12)(q36;p13) AML cases.[4-7] However, all AML cases with t(7;12)(q36;p13) have high expression of *MNX1*,[5] suggesting a yet unknown mechanism of *MNX1* activation. Consistent with the activation of a silenced gene locus, a translocation of the *MNX1* locus from the nuclear periphery to the internal nucleus was seen, an observation that is in line with the idea that condensed and silent chromatin is located in the nuclear periphery.[6] Furthermore, interactions of *ETV6* downstream elements with the *MNX1* locus have been postulated as possible mechanisms for *MNX1* activation.[6,8] The first clue for the existence of possible aberrant promoter-enhancer interactions leading to *MNX1* activation came from our investigations of the GDM-1 AML cell line, which harbors a t(6;7)(q23;q36) translocation. In GDM-1, the *MNX1* promoter interacts with an enhancer element from the *MYB* locus on chr6q23.[9]

Recently, Nilsson et al. reported the introduction of a translocation between chr7q36 and chr12p13, modeling the one found in t(7;12)(q36;p13) AML, into the human induced pluripotent stem cell (iPSC) line, ChiPSC22^{WT}.[8] The derivative line, ChiPSC22$^{t(7;12)}$, can be differentiated into hematopoietic stem and progenitor cells (HSPCs) and, as such, expresses *MNX1*, suggesting that hematopoietic enhancers play a role in *MNX1* activation. Enhancer hijacking has initially been described as a mechanism for oncogene activation in AML with inv(3)/t(3;3)(q21q26) AML, in which activation of *EVI1*, an isoform encoded from the *MDS and EVI1 complex locus* (*MECOM*), results from the repositioning of a *GATA2* enhancer.[10-12] Enhancer hijacking is also implicated in acute leukemia of ambiguous lineage in which translocated hematopoietic enhancers from different chromosomes are involved in activating *BCL11B*.[13]

Here, we provide a detailed description of the molecular alterations found in 6 patients with t(7;12)(q36;p13) AML and dissect the molecular mechanism leading to *MNX1* activation through the use of CRISPR-engineered ChiPSC22$^{t(7;12)}$ iPSCs and HSPCs. We identified that a previously proposed[8] enhancer-hijacking event activates the *MNX1* promoter via hematopoietic enhancers from the *ETV6* locus and validated this event in the iPSC/HSPC system. Our data suggest that enhancer hijacking may be a more widespread, but so far largely unappreciated, mechanism for gene activation in AML with cytogenetic abnormalities.

Methods

Samples and cell lines

Pediatric leukemia samples T1, T2, and T3 (supplemental Table 1) were obtained at diagnosis after informed consent of patients' legal guardians in accordance with the institution's ethical review board (University Essen and Medical University Hannover, MHH, no. 2899). Sample T4 (supplemental Table 1) came from a pediatric AML cohort in Gothenburg, Sweden, and informed consent was obtained from the legal guardians in accordance with the local ethical review board. Human iPSC line ChiPSC22 (Cellartis/Takara Bio Europe AB) was cultivated in the feeder-free DEF-CS system (Cellartis/Takara Bio Europe) under standard conditions. Before differentiation, cells were transferred to Matrigel (Corning) and mTeSR1 medium (STEMCELL Technologies Inc) for 2 to 3 passages. ChiPSC22 was authenticated; this line and its derivatives were regularly tested for mycoplasma contamination using a commercial test kit (VenorGeM Classic, Minerva Biolabs).

Differentiation to hematopoietic cells

Differentiation of ChiPSC22 was done as previously described.[8]

Whole-genome sequencing (WGS)

Genomic DNA was isolated using the Quick DNA Miniprep kit (Zymo Research), and libraries were sequenced in an Illumina HiSeq X Ten sequencer. FASTQ files were aligned with the Burrows-Wheeler Aligner (maximal exact match option) to the hg19 reference genome. Single nucleotide variants (SNVs) were called using mutect2. Because of the lack of matched germ line sequences, only 52 known AML driver genes (supplemental Table 2) were screened for mutations. Structural variants (SVs) and somatic copy number alterations (SCNAs) were called using the Hartwig Medical Foundation (HMF) pipeline (https://github.com/hartwigmedical/hmftools). HMF tools were used in tumor-only mode, and putative germ line SVs were filtered out using a large panel of HMF-provided normals. SVs <20 kb were filtered out. Processed data of 2 samples of the TARGET-AML data set (supplemental Table 1; database of Genotypes and Phenotypes (dbGaP) accession: phs000465.v22.p8) was downloaded using the Globus platform.[14]

RNA isolation, sequencing, and quantitative Reverse Transcriptase-Polymerase Chain Reaction (qRT-PCR)

Total RNA was isolated using the RNeasy Plus Mini kit (Qiagen). After library preparation, RNA was sequenced on NOVASEQ 6000 with 100-bp paired end. The FASTQ files were processed using the nf-core[15] RNA-sequencing (RNAseq) v3.9 pipeline, with alignment performed using Spliced Transcripts Alignment to a Reference (STAR)[16] and quantification performed with Salmon.[17] Allele-specific expression was examined by first detecting heterozygous single-nucleotide polymorphisms in exons using the genomic analysis toolkit (GATK) HaplotypeCaller and then counting the allelic expression in RNA using GATK ASEReadCounter.[18] Differential expression analysis was performed using limma for Affymetrix array data and pydeseq2 for RNAseq data.

qRT-PCR was performed as previously described using TaqMan Universal Master Mix II with uracil-N-glycosylase (ThermoFisher Scientific, Applied Biosystems) and TaqMan gene expression assays

(ThermoFisher Scientific, Applied Biosystems; supplemental Table 3).[8]

Detection of fusion transcripts

For our own samples, fusion transcripts were detected using STAR-Fusion v1.10.1.[19] For the TARGET-AML cohort, we downloaded the processed STAR-Fusion results from the Genomic Data Commons data portal.

Protein extraction, western blotting, and protein detection

Protein extraction, western blotting, and protein detection with antibodies (supplemental Table 4) was done as described previously.[9]

Expression screens

RNAseq expression data were downloaded from the TARGET cohort[20] (both TARGET-NCI (Therapeutically Applicable Research to Generate Effective Treatments, National Cancer Institute) and TARGET-FHCRC (Fred Hutchinson Cancer Research Center); https://target-data.nci.nih.gov/Public/AML/mRNA-seq/L3/expression/BCCA/). *MNX1* is not expressed in normal hematopoietic cells; hence, in RNAseq, a *MNX1* expression >0.5 transcripts per million was considered overexpression. Gene expression data files of the Balgobind cohort[21] were downloaded from Gene Expression Omnibus (GSE17855) and normalized using the affy R package (https://bioconductor.org/packages/release/bioc/html/affy.html). Log-expression values of microarray data were assumed to be normally distributed. We computed the mean and standard deviation for *MNX1* expression across all samples; those whose *MNX1* expression was higher than the mean plus 3 standard deviations were considered to express *MNX1* (3-sigma rule).

4C

Circular chromosome conformation capture (4C) with 2 million cells was done and analyzed as described[9] using *Hin*dIII in combination with *Dpn*II (supplemental Table 5).

High-throughput chromosome conformation capture (Hi-C)

Hi-C libraries were prepared and analyzed as previously described[22] with minor modifications. One million cells were fixed at a final concentration of 1% formaldehyde in RPMI 1640 medium. Digestion was performed using *Dpn*II. Two to 3 Hi-C library replicates per sample were sequenced with 240 million reads per replicate. The FASTQ files were processed using the nf-core/hic v.2.1.0 pipeline. Hi-C figures were generated using figeno (https://github.com/CompEpigen/figeno)[23].

Two-color fluorescence in situ hybridization (FISH)

Two NOVA-probe sets targeting *MNX1* (chr7:156802250-156807250) and *ETV6* (chr12:11949500-11954500) carrying multiple ATTO594 or ATTO647N dyes were synthesized as described previously[24] (supplemental Table 6). Two-color FISH was conducted as previously described with minor adaptations.[25,26] ChiPSC22$^{t(7;12)}$ iPSCs were seeded on DEF-CS COAT-1–coated coverslips (Cellartis, Takara BioSciences) and ChiPSC22$^{t(7;12)}$ HSPCs on poly-L-lysine–coated coverslips. After washing and fixation steps, coverslips were mounted on microscopic slides with Mowiol (2.5% 1,4-Diazabicyclo[2.2.2]octane and pH 7.0; Carl Roth), dried for 30 minutes, and sealed with nail polish.[27] Automated Stimulated Emission Depletion (STED) microscopy was performed according to Brandstetter et al.[25] FISH signals within confocal scans were detected using a Laplacian-of-Gaussian blob detector and subsequently imaged using 3-dimensional (3D) STED settings. Subpixel localization of FISH spots in both channels was performed by fitting a multidimensional Gaussian function plus a constant background using the Levenberg-Marquardt algorithm. The peak height of the fitted Gaussians was used to determine spot intensity. Only distances <600 nm were considered.

ACT-seq and ATAC-seq

Genome-wide targeting and mapping of histone modifications (supplemental Table 4) and mapping of open chromatin were done by antibody-guided chromatin tagmentation sequencing (ACT-seq) and assay for transposase-accessible chromatin by sequencing (ATAC-seq), respectively, as described previously.[9] For read normalization using spiked-in yeast DNA in ACT-seq, trimmed reads were additionally aligned against the *Saccharomyces cerevisiae* R64 reference genome followed by postalignment filtering. An ACT-seq library–specific scaling factor was obtained by calculating the multiplicative inverse of the number of filtered alignments against the yeast genome.[9] ACT-seq peak calling was done applying MACS v.2.2.6 (https://pypi.org/project/MACS2/) with a q-value cutoff of 0.05 and default parameters using a wrapper script with settings narrowPeak and broadPeak for acetylated lysine 27 of histone 3 (H3K27ac) and (monomethylated lysine 4 of histone 3) H3K4me1, respectively. To facilitate visualization of hematopoietic-specific enhancers in the Integrative Genomics Viewer (version 2.11.7),[28] we generated HSPC-specific H3K27ac and H3K4me1 bw-tracks with callpeaks using corresponding iPSC data as internal reference.

Deletion of the enhancer region

A region of 213.5 kb (chr12:11951022-12164578, GRCh37/hg19) covering the 4 enhancers located closest to the break point in ChiPSC22$^{t(7;12)}$ was deleted by CRISPR/Cas9 editing as described previously[8] using CRISPR RNAs designed with the Alt-R Custom Cas9 crRNA Design Tool (Integrated DNA Technologies). To join the 2 ends by homology-directed repair, a 150 single-stranded deoxynucleotide was designed with 75 bases sequence homology on each side. Deletion was done in ChiPSC22^{WT} and ChiPSC22$^{t(7;12)}$ sublines 14D7 and 24C7.[8] The presence of the deletion on the translocated and the wild-type allele was validated by PCR using the Terra PCR Direct Polymerase Mix (Takara Bio Europe; supplemental Table 7). From line 14D7, cell line 2304B4 was generated, and from 24C7, lines 2305B10 and 2305C9 were generated.

Phenotypic characterization of enhancer deletion clones

For flow cytometry analysis, cells were resuspended in phosphate-buffered saline plus EDTA and incubated with the mix of antibodies for 15 to 20 minutes in the dark at room temperature. Cells were washed once and resuspended in phosphate-buffered saline plus

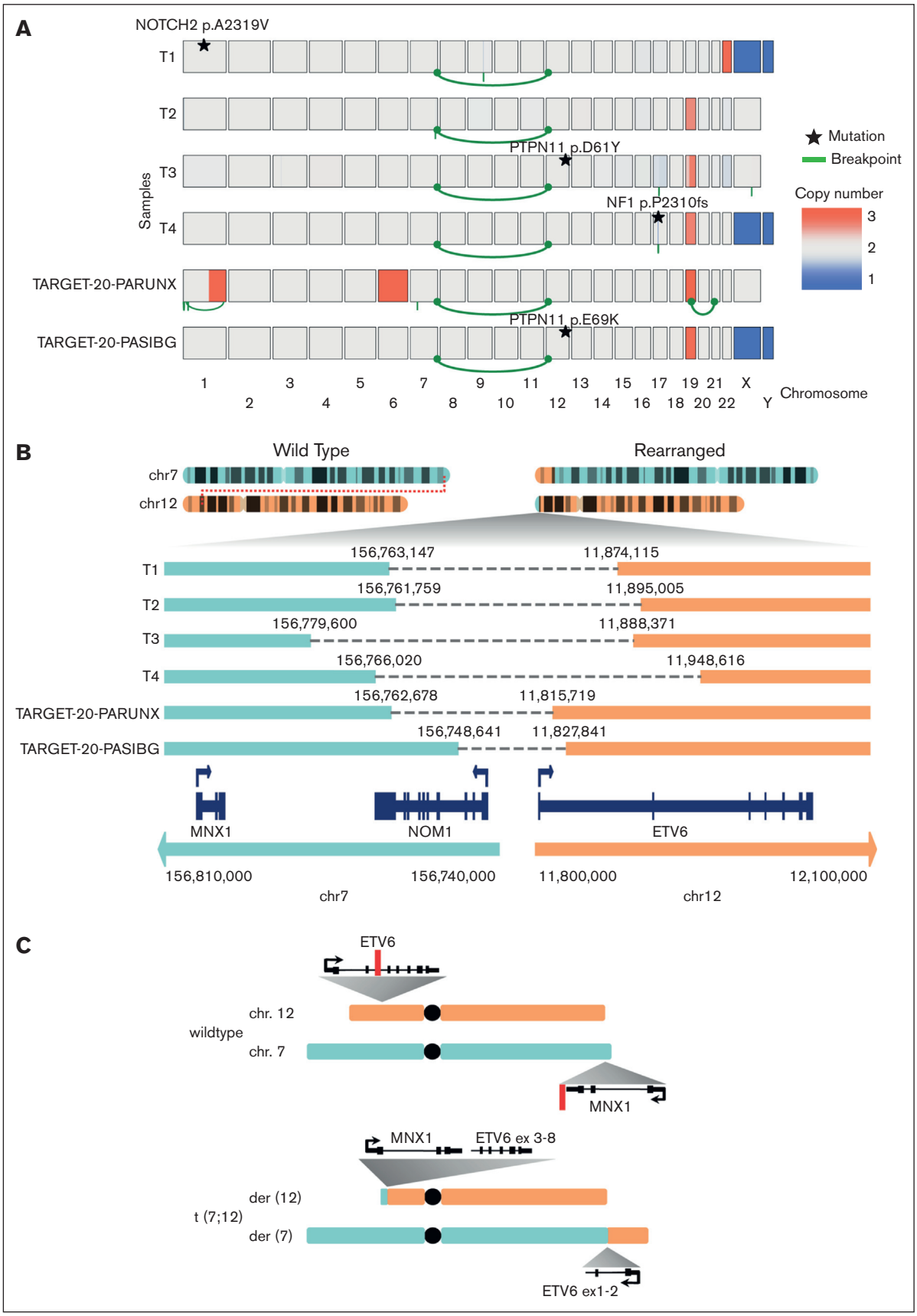
A
NOTCH2 p.A2319V
T1
T2
PTPN11 p.D61Y
T3
NF1 p.P2310fs
T4
Samples
TARGET-20-PARUNX
PTPN11 p.E69K
TARGET-20-PASIBG
Mutation
Breakpoint
Copy number
3
2
1
1 2 3 4 5 6 7 8 9 10 11 12 13 14 15 16 17 18 19 20 21 22 X Y
Chromosome
B
Wild Type
Rearranged
chr7
chr12
156,763,147
11,874,115
T1
156,761,759
11,895,005
T2
156,779,600
11,888,371
T3
156,766,020
11,948,616
T4
156,762,678
11,815,719
TARGET-20-PARUNX
156,748,641
11,827,841
TARGET-20-PASIBG
MNX1
NOM1
ETV6
156,810,000
156,740,000
chr7
11,800,000
12,100,000
chr12
C
ETV6
chr. 12
wildtype
chr. 7
MNX1
MNX1
ETV6 ex 3-8
der (12)
t (7;12)
der (7)
ETV6 ex1-2

Figure 1.

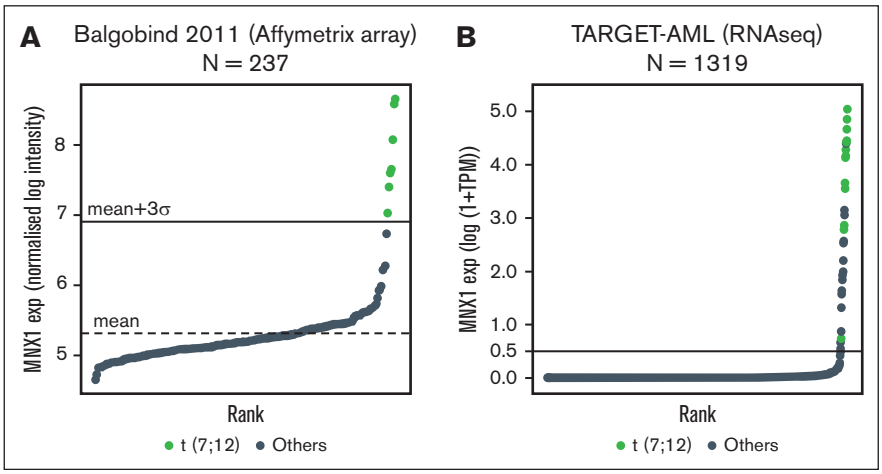

Figure 2. *MNX1* expression in pediatric AML with t(7;12)(q36;p13) translocation. (A-B) *MNX1* expression in 2 different pediatric AML cohorts. (A) Balgobind et al[31]; 237 samples profiled with Affymetrix arrays. The mean expression level is shown with a dashed line, and the mean plus 3 standard deviations is shown with a horizontal line. (B) TARGET-AML[29]; 1319 samples profiled with RNAseq (cutoff, 0.5 TPM). Samples with cytogenetically detected t(7;12)(q36;p13) translocation are shown in green and other samples in gray. exp, expression; TPM, transcripts per million.

EDTA. Data were collected on BD FACS Aria (BD Biosciences) and analyzed using BD FACSDiva. The colony-forming unit assay was done using MethoCult H4034 Optimum (STEMCELL Technologies) following the manufacturer's protocol. Proliferation was analyzed by continuous culture of the HSPCs in StemSpan SFEM II + CC100 (STEMCELL Technologies) for 14 days. Cells were counted every 48 hours, centrifuged, and 75% fresh medium was added to 25% old medium. Cell division was calculated as follows: ln(B/A)/(ln2), in which A = number of seeded cells and B = number of cells after 48 hours.

Results

WGS of t(7;12)(q36;p13) AML

To precisely map structural rearrangements, SCNAs, and genetic mutations in t(7;12)(q36;p13) AML, we performed WGS of 4 t(7;12)(q36;p13) AML cases, T1, T2, T3, and T4 (Figure 1A; supplemental Table 1). We additionally used published WGS data from 2 samples with t(7;12)(q36;p13) from the TARGET cohort[29] (supplemental Table 1). The presence of t(7;12)(q36;p13) as a reciprocal balanced translocation was verified in all 6 samples (Figure 1A). The break point on chr12 is located in 5 samples in intron 1 and in 1 sample in intron 2 of ETV6. On chr7, all break points are located proximal to *MNX1*; in 4 cases within *NOM1*, located next to *MNX1*; and in 2 cases, between *MNX1* and *NOM1* (Figure 1B). In none of these cases, an oncofusion gene between *MNX1* and *ETV6* is supported by the observed translocation break points, leaving the main *MNX1* variant (RefSeq: NM_005515) unaffected by the genomic rearrangements (Figure 1C). Accompanying cytogenetic data (supplemental Table 1) revealed trisomy 19 in all cases, a result confirmed by SCNA analysis for all cases except for T1, for which SCNA analysis identified a trisomy 22 but no trisomy 19 (Figure 1A). We found mutations in common leukemia genes (supplemental Table 2), namely in *NOTCH2* (p.A2319V), *NF1* (p.P2310fs), and *PTPN11* (p.D61Y and p.E69K; Figure 1A).

T1, T2, and T3 were profiled with RNAseq, but no fusion transcript *MNX1*::*ETV6* could be identified. The TARGET-AML cohort contains 14 t(7;12) samples, and of these, only 1 has an *MNX1*::*ETV6* fusion detected by STAR-Fusion (TARGET-20-PAWNHH), and 1 has an *ETV6*::*LMBR1* fusion (TARGET-20-PAWNYK). Therefore, fusion transcripts do not appear to be the driving factor behind t(7;12)(q36;p13).

MNX1 is highly expressed in all t(7;12)(q36;p13) AML and is associated with a characteristic gene expression signature

Although normally not expressed in the hematopoietic lineage, *MNX1* is highly expressed in all analyzed t(7;12)(q36;p13) AML.[5,6,30] In line with this, AML cases T1 to T4 showed high *MNX1* expression (supplemental Table 1). We additionally evaluated *MNX1* expression in 2 pediatric AML cohorts with available expression data: Balgobind et al (237 samples profiled with Affymetrix array[31]; Figure 2A) and TARGET-AML (1319 samples profiled with RNAseq[29]; Figure 2B). *MNX1* was expressed in 7 of 237 samples (2.9%) of the Balgobind cohort and in 31 of 1319 (2.3%; including resample for samples TARGET-20-PARUNX and TARGET-21-PASVJS) samples of the TARGET-AML cohort. All t(7;12) samples showed *MNX1* expression but also some samples without 7q36-rearrangements. Accordingly, there might be alternative mechanisms leading to *MNX1* activation. Most t(7;12)(q36;p13) samples were diagnosed at younger than 2 years; however, most *MNX1*-overexpressing samples without t(7;12) were diagnosed at an older age (supplemental Table 1). A characteristic gene expression signature for t(7;12)(q36;p13) AML compared with other cytogenetic subgroups in pediatric AML has been described.[31] The majority of these genes are either

Figure 1. WGS analysis of t(7;12)(q36;p13) AML. (A) Copy numbers (blue, loss; red, gain), structural rearrangements (green bow connecting 2 chromosomes), and mutations in known AML driver genes for 6 t(7;12)(q36;p13) AML samples based on WGS. Samples T1, T2, T3, and T4 were profiled in this study, whereas TARGET-20-PARUNX and TARGET-20-PASIBG are from the TARGET-AML cohort 15. (B) Sketch of the rearranged chr7 and chr12 and zoom-in on the region around the break points. (C) Schematic overview of chr7 (turquoise), chr12 (orange), and derivative chromosomes der(12) and der(7) resulting from the reciprocal t(7;12) translocation involving *MNX1* on chr7 and *ETV6* on chr12. Red lines indicate positions of break/fusion points.

consistently downregulated in t(7;12)(q36;p13) AML (eg, *TP53BP2*) or upregulated together with *MNX1* (*EDIL3, LIN28B, BAMBI, MAF, FAM171B, AGR2, CRISP3, KRT72*, and *MMP9*). These do not lie on the translocated piece of chr7; and, hence, their expression change might be a secondary effect of the translocation. We performed differential expression analysis between the t(7;12)(q36;p13) and the other cases from each the Balgobind and the TARGET-AML cohort (supplemental Table 8; supplemental Figure 1). Our lists of upregulated and downregulated genes include the genes identified by Balgobind et al,[31] which are indeed consistently deregulated in t(7;12)(q36;p13) across several cohorts, as well as other genes not reported before. The samples with *MNX1* expression but without genomic rearrangement close to *MNX1* did not exhibit this typical gene signature (supplemental Figures 1 and 2). Several experimental systems have recently been developed to model t(7;12): an HSPC system with a t(7;12) translocation[8,32] and a mouse model of leukemia induced by *MNX1* overexpression.[33] The HSPC system partially recapitulated the patients' gene expression signature, whereas in the mouse model, most genes of the t(7;12) signature were not differentially expressed (supplemental Figure 2).

The break points on chr12 in the t(7;12)(q36;p13) samples led to a corrupted *ETV6* allele and reduced *ETV6* expression compared with other samples (supplemental Figure 3), but this was not significant due to the low number of t(7;12) cases and the high *ETV6* expression variability even in the absence of rearrangements. Heterozygous single-nucleotide polymorphisms in exons of *ETV6* were found in T1 and T3, and the allele frequency in RNA suggested monoallelic expression of ETV6 in the leukemic cells (supplemental Figure 3).

A t(7;12)(q36;p13) cell line model exhibits *MNX1* protein expression and chromatin interactions between the *MNX1* and *ETV6* regions

Previously, Nilsson et al engineered an iPSC line harboring a balanced translocation t(7;12)(q36;p13) (ChiPSC22$^{t(7;12)}$) with a break point in *ETV6* intron 2 and a second one ~21 kb proximal to *MNX1* in the common break point region.[8,32] Upon differentiation of ChiPSC22$^{t(7;12)}$ cells to HSPCs, *MNX1* became activated. We confirmed this result at the protein level in 3 ChiPSC22$^{t(7;12)}$ sublines, 14D7, 23G8, and 24C7; the *MNX1* protein was only expressed in the ChiPSC22$^{t(7;12)}$ HSPCs but not in the ChiPSC22$^{t(7;12)}$ iPSCs, ChiPSC22^{WT} iPSCs or ChiPSC22^{WT} HSPCs (Figure 3A). WGS of the 3 sublines did not reveal any relevant changes to the original line ChiPSC22, except for the presence of the heterozygous t(7;12). To examine whether the t(7;12)(q36;p13) translocation juxtaposes enhancers from the *ETV6* region with the *MNX1* promoter, we profiled the iPSCs and HSPCs of both ChiPSC22^{WT} and ChiPSC22$^{t(7;12)}$ lines with Hi-C. No interactions were seen between chr7 and chr12 in the ChiPSC22^{WT} (supplemental Figure 4), but we observed a new topologically associating domain (neo-TAD) around the break point in both iPSC and HSPC ChiPSC22$^{t(7;12)}$ (Figure 3B). The neo-TAD extends up to chr12:12200000, meaning that enhancers located between the break point and the end of the neo-TAD could interact with the *MNX1* promoter. Public ChIPseq data from K562 cells revealed binding of CCCTC-Binding Factor (CTCF) and *Radiation Gene 21* (RAD21) at the extremities of the neo-TAD, which would explain its formation (Figure 3B). For an independent proof of interaction, we performed 4C using an *MNX1* viewpoint (chr7:156805780-156806574) and a viewpoint located in the neo-TAD, close to the *ETV6* break point (chr12:11953871-11954315; supplemental Table 5). Reciprocal 4C confirmed the interaction between the *MNX1* and *ETV6* regions in HSPCs and, less strongly, in 1 iPSC sample (supplemental Figure 5).

We further performed 2-color FISH targeting the *MNX1* promoter and a neo-TAD region located close to the *ETV6* break point and observed a significantly decreased 3D distance between the targeted regions in ChiPSC22$^{t(7;12)}$ HSPCs compared with the corresponding iPSCs (Figure 3C). This suggests a reinforced contact between an enhancer from the *ETV6* neo-TAD region and the *MNX1* promoter upon differentiation.

Identification of hematopoietic enhancers in *ETV6* and its vicinity

We next searched for hematopoietic enhancers located in the chr12 part of the neo-TAD. Active enhancers reside in open chromatin; hence, we profiled accessible chromatin by ATAC in AML-T1 and -T2 and in HSPCs of our cell line model. The patient samples clustered with the HSPCs, separately from the iPSCs, and had similar peaks as HSPCs (supplemental Figure 6A-B). We found 4 consistent open chromatin sites common to the patient samples and to the ChiPSC22$^{t(7;12)}$ and ChiPSC22^{WT} cells within the ETV6 neo-TAD (Figure 4). Additionally, we mapped peaks of enhancer marks H3K27ac and H3K4me1 in both iPSCs and HSPCs. To facilitate the identification of hematopoietic enhancers in ChiPSC22$^{t(7;12)}$ and ChiPSC22^{WT} HSPCs, we applied MACS2 peak calling using the corresponding iPSC data as internal reference. The 4 open chromatin regions were also marked by HSPC-specific H3K27ac and H3K4me1 peaks. In addition, we used public chromatin immunoprecipitation followed by sequencing (ChIPseq) data sets for the same enhancer marks (Gene Expression Omnibus: GSM772885 and GSM621451) and the histone acetyltransferase P300, generated from CD34^{+} cells and the chronic myeloid leukemia–derived cell line MOLM-1.[10] Again, the 4 ATAC/H3K27ac/H3K4me1 peaks were found as well in MOLM-1 and CD34^{+} cells (Figure 4). Two of these peaks coincide in addition with p300 peaks (Figure 4). In conclusion, we identified 4 strong enhancer candidates in the *ETV6* neo-TAD region, 2 of which coincide with p300 peaks and may drive *MNX1* activation in t(7;12)(q36;p13) AML.

Deletion of enhancers in the *ETV6* region abrogates *MNX1* expression in ChiPSC22$^{t(7;12)}$ HSPCs

As a further layer of experimental evidence for de novo promoter-enhancer interactions in t(7;12)(q36;p13) AML, we examined *MNX1* expression levels in 3 ChiPSC22$^{t(7;12)}$ sublines carrying a deletion of 213.5 kb, which removed the 4 enhancer candidates (ChiPSC22$^{t(7;12)\Delta En}$; Figure 5A; supplemental Figure 7A). We performed WGS of the ChiPSC22$^{t(7;12)\Delta En}$ derivatives 2304B4 and 2305C9, could confirm the enhancer deletion in both, and found no other rearrangements in 2304B4 but an inversion in the nontranslocated *ETV6* allele of 2305B9 (supplemental Figure 8). Consequently, clone 2305B9 was omitted from further analyses. In the other 2 ChiPSC22$^{t(7;12)\Delta En}$ lines, HSPC-specific *MNX1*

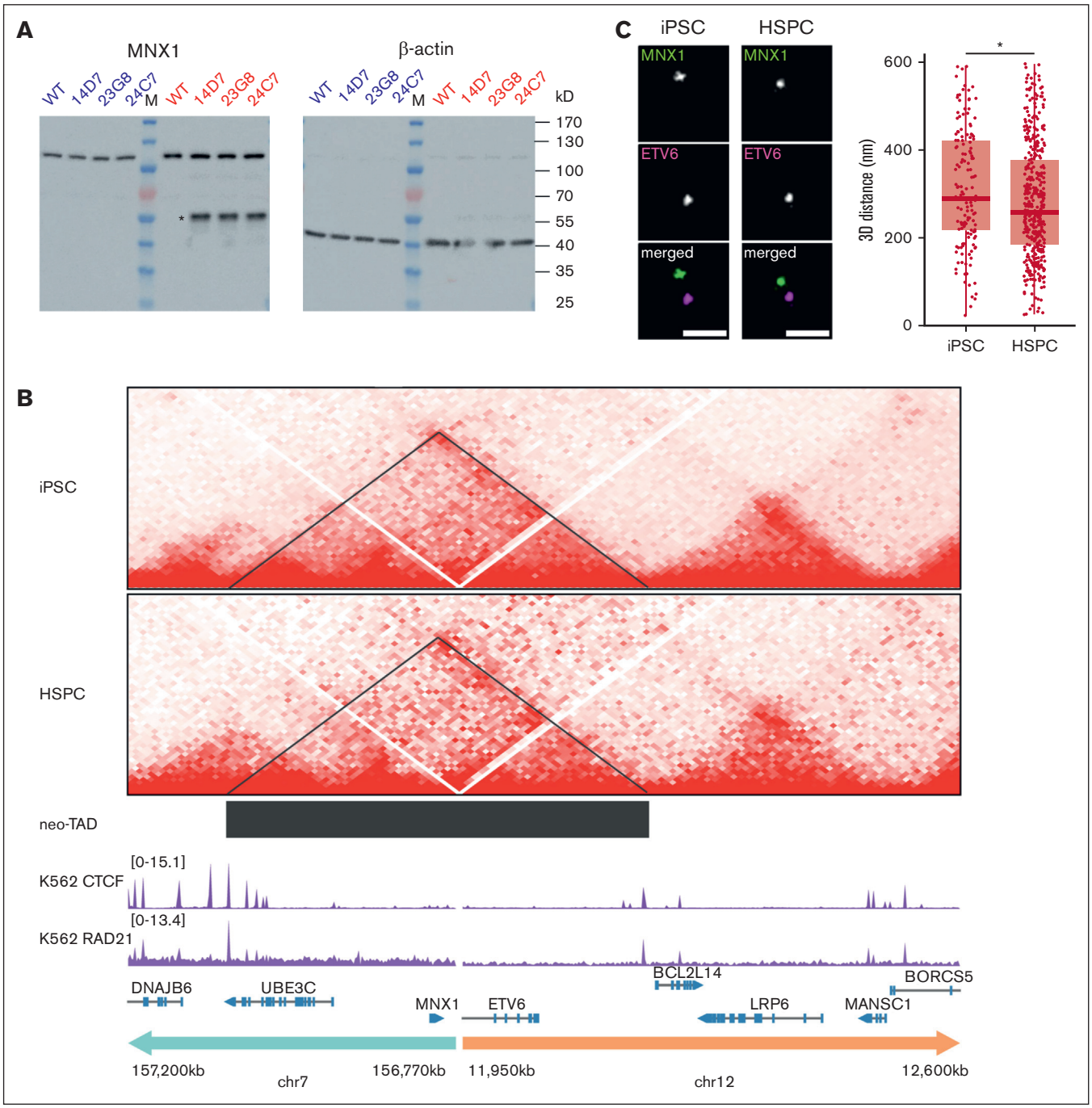

Figure 3. MNX1 protein expression and chromatin interaction of the *MNX1* gene with the *ETV6* region in ChiPSC22$^{t(7;12)}$ cells. (A) Western blot with an *MNX1* antibody (left) and iPSC (blue) and HSPC (red) protein extracts from ChiPSC22^{WT} and ChiPSC22$^{t(7;12)}$ sublines 14D7, 23G8, and 24C7. The *MNX1* protein (asterisk) is only detected in HSPCs of ChiPSC22$^{t(7;12)}$ sublines 14D7, 23G8, and 24C7. The common band at ~120 kD results from an unknown protein cross-reacting with the *MNX1* antibody. To demonstrate loading of equal protein amounts, the unstripped blot was reincubated with an antibody against β-actin (right). (B) Chromatin interactions analyzed by Hi-C seq in the genomic region flanking the translocation break point in the ChiPSC22$^{t(7;12)}$ subline 24C7, either as iPSCs (top) or HSPCs (below). The neo-TAD is indicated by a black bar. ChIPseq data for CTCF and RAD21 in K562 were retrieved from the encode project (IDs ENCFF468HJA and ENCFF000YXZ). (C) Increased proximity between *MNX1* and *ETV6* in ChiPSC22t(7;12) subline 14D7–derived HSPCs compared with iPSCs. Representative STED images of FISH spots in 2 colors targeting *MNX1* and *ETV6* in iPSCs and HSPCs (left). Scale bars, 500 nm. 3D distances between the *MNX1* and *ETV6* signals (right). Red horizontal lines within boxes indicate medians; box limits indicate upper and lower quartiles. iPSCs, n = 154; HSPCs, n = 409, across 3 independent replicates. *$P < .05$, Wilcoxon rank-sum test.

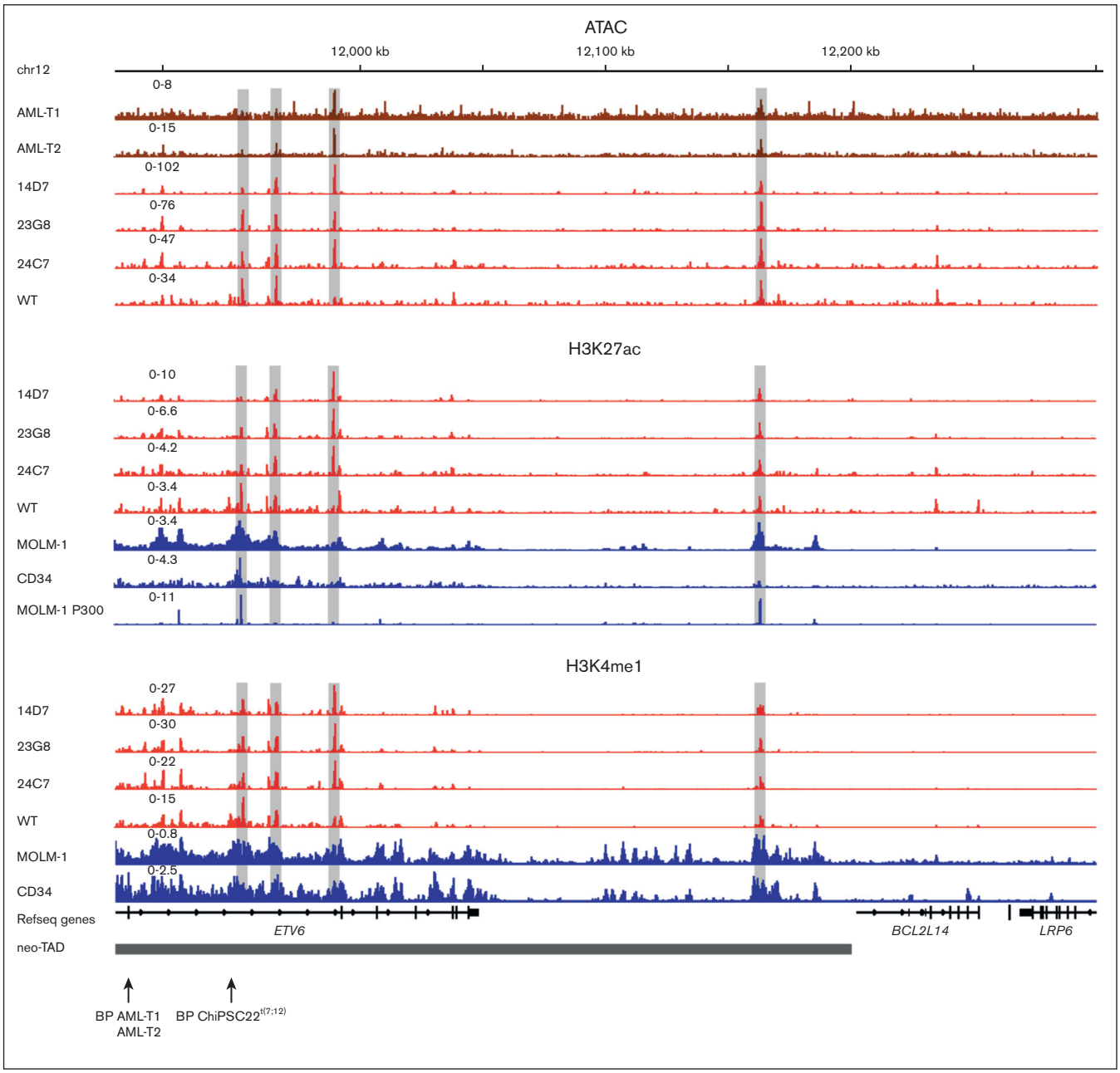

Figure 4. Open chromatin and enhancer mark profiles in the *ETV6* neo-TAD region of patient and cell line samples. Open chromatin profiles (ATAC) of patients with AML , T1 and T2, and of HSPCs from ChiPSC22^{WT} and ChiPSC22$^{t(7;12)}$ sublines 14D7, 23G8, and 24C7 in the *ETV6* neo-TAD region. HSPC-specific enhancer mark H3K27ac and H3K4me1 profiles and publicly available[10] p300, H3K27ac, and H3K4me1 profiles from MOLM-1 and CD34^{+}. Relevant common peak positions are highlighted by a gray shading. The chr12 break point (BP) position in T1 and T2 and in the ChiPSC22$^{t(7;12)}$ sublines are indicated.

expression was abrogated (Figure 5B), whereas the expression of *LRP6* and *BCL2L14* near the deletion was not changed (supplemental Figure 7B). This supports the hypothesis that *MNX1* activation in ChiPSC22$^{t(7;12)}$ is the result of interactions between the *MNX1* promoter and 1 or multiple enhancers located in or close to *ETV6*. We also observed downregulation of genes that are upregulated together with *MNX1* in t(7;12)(q36;p13), such as *AGR2, MMP9, MAF*, and *CRISP3* (Figure 5B), suggesting that they are regulated by *MNX1*. Similar to differentiated ChiPSC22^{WT}, *ETV6* was upregulated, which might be explained by *MNX1* regulation as well. Further phenotypic characterization of the ChiPSC22$^{t(7;12)\Delta En}$ sublines 2304B4 and 2305B10 revealed that there is no difference in differentiation capacity compared with the parental ChiPSC22$^{t(7;12)}$ (supplemental Figure 7C). The HSPCs derived from both groups also show similar proliferation rates and give rise to similar colony-forming units (supplemental Figure 7D-E).

In conclusion, we provide experimental evidence for a previously proposed enhancer-hijacking event[8] rather than the creation of an oncofusion protein in pediatric AML with t(7;12)(q36;p13). Using

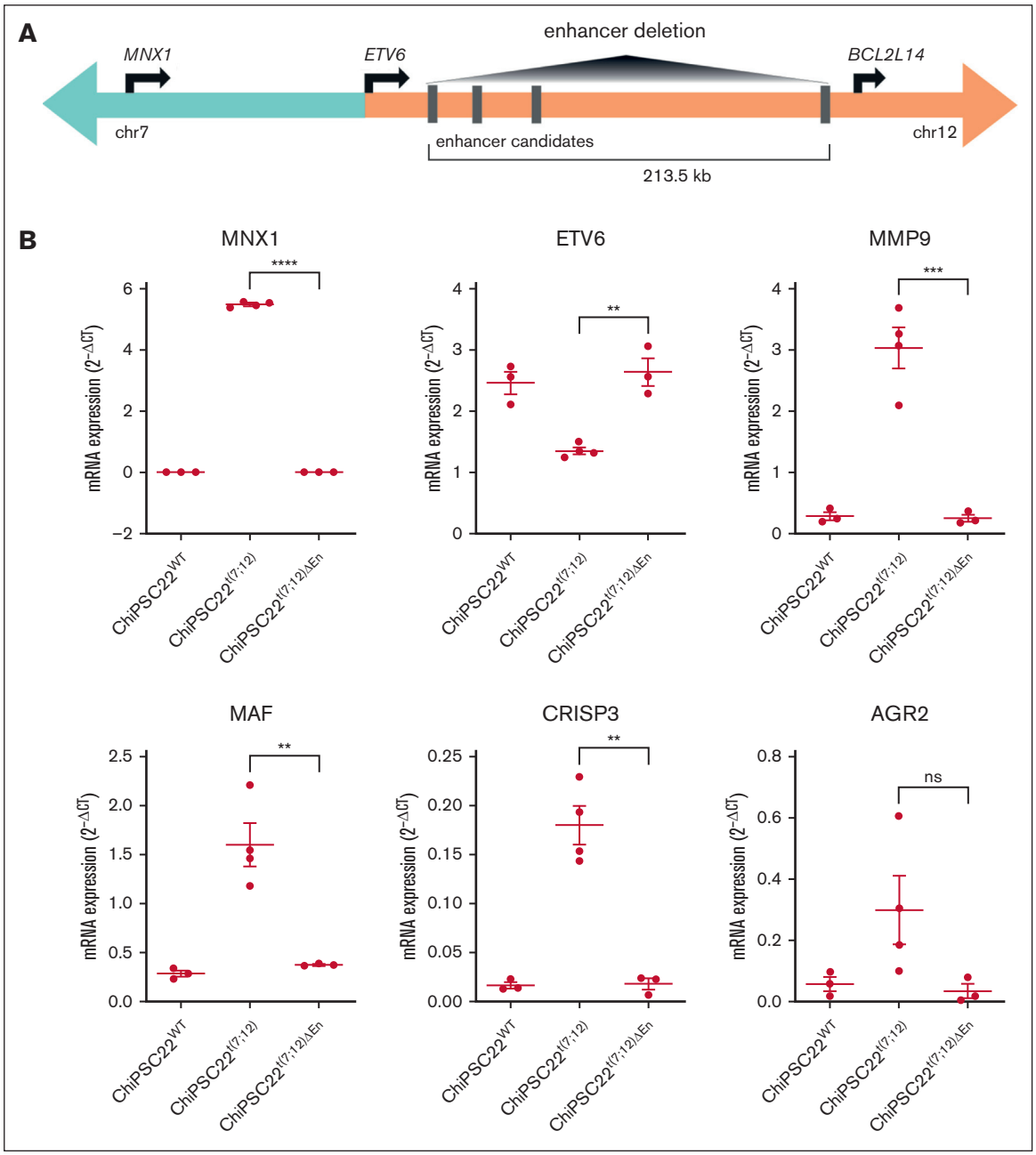

Figure 5. Molecular validation of enhancer-promoter interaction in ChiPSC22$^{t(7;12)}$ upon differentiation. (A) Scheme of the enhancer deletion experiment performed to validate the interaction between the *MNX1* promoter and enhancers distal to the BP. (B) Gene expression in HSPCs derived from ChiPSC22^{WT} (n = 3), ChiPSC22$^{t(7;12)}$ (n = 4, from 2 independent cell lines), and ChiPSC22$^{t(7;12)\Delta En}$ (n = 3, from 2 independent cell lines) measured via qRT-PCR and shown as $2^{-\Delta Ct}$ vs *GUSB* as endogenous reference. ****$P < .0001$; ***$P < .001$; **$P < .01$; *$P < .05$. ns, not significant.

an in vitro iPSC/HSPC cell system, we demonstrate that 1 or several enhancers in the *ETV6* region interact with *MNX1* to regulate its expression.

Discussion

In this manuscript, we describe enhancer hijacking and activation of *MNX1* as a novel molecular mechanism resulting from a translocation between chr7 and chr12 [t(7;12)(q36;p13)] in pediatric AML. Our study shifts the focus from a putative *MNX1*::*ETV6* oncofusion transcript[42] to the activation of *MNX1* as the unifying putative leukemia-driving event. Overexpression of *MNX1* is accompanied by monoallelic inactivation of *ETV6* on the translocated chromosome, putatively resulting in haploinsufficiency. Our observation has important implications for the diagnosis of this subgroup of patients, as well as novel therapeutic approaches. As shown in the expression reanalysis, all t(7;12)(q36;p13) AML demonstrate overexpression of *MNX1*. Only few AML cases without t(7;12)(q36;p13) show *MNX1* overexpression; but although t(7;12)(q36;p13) AML is diagnosed at a very young age

(<20 months), *MNX1* overexpression in the absence of this translocation occurs predominantly at a later age, suggesting different, yet unexplained, molecular pathways converging in *MNX1* expression. Considering that *MNX1* is not expressed in the normal hematopoietic system, quantitative *MNX1* expression analysis could be used as a diagnostic marker for this subgroup of pediatric AML.

Enhancer-hijacking events resulting in the activation of proto-oncogenes have been described also in other human malignancies including translocations resulting in the activation of oncogenes *MYC, BCL2*, or *CCND1* in B-cell lymphoma[34-36] or rearrangements in medulloblastoma.[37] Subtype-specific 3D genomic alterations were recently discovered in AML leading to enhancer-promoter or enhancer-silencer loops.[38] We demonstrated that the t(7;12)(q36;p13) translocation results in a neo-TAD, in which the *MNX1* promoter is able to interact with the *ETV6* region.

Initial evidence for an oncogenic role of *MNX1* in leukemogenesis comes from a study by Nagel et al characterizing the *MNX1*-overexpressing cell line GDM-1.[20] Knockdown of *MNX1* led to a reduction of cell viability and cell adhesion. In vitro overexpression of *MNX1* in HT1080 and NIH3T3 cells leads to premature, oncogene-induced senescence mediated by the induction of p53 signaling.[39] In vivo, ectopic *MNX1* expression in murine HSPCs resulted in strong differentiation arrest and accumulation at the megakaryocyte/erythrocyte progenitor stage.[39] Overall, this phenotype is in line with reports on t(7;12)(q36;p13) AML blast cells that are less differentiated (French-American-British subtype M0 or M2) and demonstrate expression of the stem cell markers CD34 and CD117.[5,40] Waraky et al used retroviral transduction of *MNX1*-expressing constructs into murine fetal HSPCs and were able to induce AML.[33] A possible link to leukemogenesis was described with the observation that *MNX1* activation resulted in reduced H3K4me1/2/3 and H3K27me3 levels providing increased chromatin accessibility.[33]

Our study challenges the concept in AML that all reciprocal translocations lead to oncofusion proteins as an overestimated molecular mechanism in AML for gene activation. Future studies unraveling the molecular defects of t(7;12)(q36;p13) AML should focus on the targets of homeobox transcription factor *MNX1* rather than the oncofusion, as already initiated in some reports.[21,30,39] Furthermore, copy number alterations of genes such as *DNA methyltransferase 1* (*DNMT1*) or *RNA polymerase II transcriptional elongation factor* (*ELL*) on chr19, coupregulation of genes such as *EDIL3* and *LIN28B*, or haploinsufficiency of *ETV6* might contribute to the leukemogenic process. ETV6 is a strong transcriptional repressor, and haploinsufficiency could result in reactivation of its target genes.[41] Moreover, the study of a potential therapeutic benefit by epigenetic drug treatment targeting *MNX1* promoter-*ETV6* enhancer interaction in the ChiPSC22$^{t(7;12)}$ iPSC/HSPC model is warranted.

We recognize that this study has several limitations that could be overcome in future studies. Due to the rarity of the disease and the limitations in obtaining primary leukemic samples, multiple (epi) genomic studies on a single patient sample are currently not possible but may become possible with improved biobanking, international collaboration, and the development of low-input profiling assays. A step in this direction is the survival analysis in pediatric AML by the NOPHO-AML.[4] Another limitation is the mapping of responsible enhancers in the 213 kb ETV6 region, including at least 4 potential hematopoietic enhancers that could drive *MNX1* expression. Individual enhancer knockout experiments will determine whether a single enhancer or multiple enhancers are required to activate *MNX1*.

Acknowledgments

The authors thank the Genomics and Proteomics Core Facility, the Omics IT and Data Management Core Facility of the German Cancer Research Center, Heidelberg, Germany, and the Center for Advanced Light Microscopy at the Ludwig-Maximilians-University Munich for their excellent support.

This work was, in part, supported by funds from the Helderleigh Foundation (Enhance Program) and German Research Foundation, SFB1074 subproject B11N (SFB1074/3 2020 Project Number:217328187 C.P. and A.R.), Carreras Foundation (DJCLS 03 R/2022 C.P. and E.S.) and FOR2674 subprojects A1 (PL 202/7-2), A6 (LI 2492/3-1), and A9 (PL 202/8-2 C.P. and D.B.L.), the Swedish Cancer Society (200925 PjF, CAN2017/461), the Swedish Childhood Cancer Foundation (PR2021-0025 and TJ2022-0017) and Västra Götalandsregionen (ALFGBG-431881 [L.P.]), and the SFB1064 subproject A17 (H.L.). Further support comes from the Helmholtz International Graduate School (A.R. and E.S.).

Authorship

Contribution: Y.L.B., G.G., B.S., D.R., and L.B. provided the clinical specimens; A.R., A.T., M.B., A.Ö., T.N., S.J., M.E., A.W., A.D., C.S., H.H., and H.L. performed the experimental procedures; E.S., U.H.T., J.H., J.A.W., K.B., J.A.W., P.L., and D.W. performed the bioinformatics and statistical analyses; E.S. was responsible for the sequence data upload to the public databases; D.B.L., L.P., D.W., and C.P. designed the study and supervised the experimental and bioinformatics work; D.W., A.R., E.S., and C.P. wrote the paper; and all authors provided feedback on the report.

Conflict-of-interest disclosure: L.B. has received honoraria from AbbVie, Amgen, Astellas, Bristol Myers Squibb, Celgene, Daiichi Sankyo, Gilead, Hexal, Janssen, Jazz Pharmaceuticals, Menarini, Novartis, Pfizer, Roche, and Sanofi; and research support from Bayer and Jazz Pharmaceuticals. D.B.L. receives honoraria from Infectopharm GmbH. The remaining authors declare no competing financial interests.

ORCID profiles: D.W., 0000-0002-7915-412X; A.R., 0000-0002-0626-3894; E.S., 0000-0002-3612-8562; U.H.T., 0009-0009-6923-6816; J.H., 0000-0003-2842-764X; K.B., 0000-0003-3716-7739; P.L., 0000-0001-9383-8555; A.W., 0000-0003-4635-021X; B.S., 0000-0001-5256-1270; C.S., 0000-0003-3590-2103; H.H., 0000-0003-1218-2107; H.L., 0000-0002-5086-6449; D.R., 0000-0002-7027-4483; L.P., 0000-0001-9274-360X; D.B.L., 0000-0001-5081-7869; C.P., 0000-0003-2554-3952.

Correspondence: Christoph Plass, Division of Cancer Epigenomics, German Cancer Research Center, INF 280, 69120 Heidelberg, Germany; email: c.plass@dkfz.de; and Daniel B. Lipka, Section of Translational Cancer Epigenomics, Division of Translational Medical Oncology, German Cancer Research Center, Im Neuenheimer Feld 581, 69120 Heidelberg, Germany; email: d.lipka@dkfz.de.

References

1. de Thé H, Pandolfi PP, Chen Z. Acute promyelocytic leukemia: a paradigm for oncoprotein-targeted cure. *Cancer Cell*. 2017;32(5):552-560.
2. Tosi S, Giudici G, Mosna G, et al. Identification of new partner chromosomes involved in fusions with the ETV6 (TEL) gene in hematologic malignancies. *Genes Chromosomes Cancer*. 1998;21(3):223-229.
3. Wlodarska I, La Starza R, Baens M, et al. Fluorescence in situ hybridization characterization of new translocations involving TEL (ETV6) in a wide spectrum of hematologic malignancies. *Blood*. 1998;91(4):1399-1406.
4. Espersen ADL, Noren-Nyström U, Abrahamsson J, et al. Acute myeloid leukemia (AML) with t(7;12)(q36;p13) is associated with infancy and trisomy 19: data from Nordic Society for Pediatric Hematology and Oncology (NOPHO-AML) and review of the literature. *Genes Chromosomes Cancer*. 2018;57(7):359-365.
5. von Bergh ARM, van Drunen E, van Wering ER, et al. High incidence of t(7;12)(q36;p13) in infant AML but not in infant ALL, with a dismal outcome and ectopic expression of HLXB9. *Genes Chromosomes Cancer*. 2006;45(8):731-739.
6. Ballabio E, Cantarella CD, Federico C, et al. Ectopic expression of the HLXB9 gene is associated with an altered nuclear position in t(7;12) leukaemias. *Leukemia*. 2009;23(6):1179-1182.
7. Beverloo HB, Panagopoulos I, Isaksson M, et al. Fusion of the homeobox gene HLXB9 and the ETV6 gene in infant acute myeloid leukemias with the t(7;12)(q36;p13). *Cancer Res*. 2001;61(14):5374-5377.
8. Nilsson T, Waraky A, Östlund A, et al. An induced pluripotent stem cell t(7;12)(q36;p13) acute myeloid leukemia model shows high expression of MNX1 and a block in differentiation of the erythroid and megakaryocytic lineages. *Int J Cancer*. 2022;151(5):770-782.
9. Weichenhan D, Riedel A, Meinen C, et al. Translocation t(6;7) in AML-M4 cell line GDM-1 results in MNX1 activation through enhancer-hijacking. *Leukemia*. 2023;37(5):1147-1150.
10. Gröschel S, Sanders MA, Hoogenboezem R, et al. A single oncogenic enhancer rearrangement causes concomitant EVI1 and GATA2 deregulation in leukemia. *Cell*. 2014;157(2):369-381.
11. Ottema S, Mulet-Lazaro R, Beverloo HB, et al. Atypical 3q26/MECOM rearrangements genocopy inv(3)/t(3;3) in acute myeloid leukemia. *Blood*. 2020;136(2):224-234.
12. Ottema S, Mulet-Lazaro R, Erpelinck-Verschueren C, et al. The leukemic oncogene EVI1 hijacks a MYC super-enhancer by CTCF-facilitated loops. *Nat Commun*. 2021;12(1):5679.
13. Montefiori LE, Bendig S, Gu Z, et al. Enhancer hijacking drives oncogenic BCL11B expression in lineage-ambiguous stem cell leukemia. *Cancer Discov*. 2021;11(11):2846-2867.
14. Foster I. Globus online: accelerating and democratizing science through cloud-based services. *IEEE Internet Comput*. 2011;15(3):70-73.
15. Ewels PA, Peltzer A, Fillinger S, et al. The nf-core framework for community-curated bioinformatics pipelines. *Nat Biotechnol*. 2020;38(3):276-278.
16. Dobin A, Davis CA, Schlesinger F, et al. STAR: ultrafast universal RNA-seq aligner. *Bioinformatics*. 2013;29(1):15-21.
17. Patro R, Duggal G, Love MI, Irizarry RA, Kingsford C. Salmon provides fast and bias-aware quantification of transcript expression. *Nat Methods*. 2017;14(4):417-419.
18. McKenna A, Hanna M, Banks E, et al. The Genome Analysis Toolkit: a MapReduce framework for analyzing next-generation DNA sequencing data. *Genome Res*. 2010;20(9):1297-1303.
19. Haas BJ, Dobin A, Li B, Stransky N, Pochet N, Regev A. Accuracy assessment of fusion transcript detection via read-mapping and de novo fusion transcript assembly-based methods. *Genome Biol*. 2019;20(1):213.
20. Nagel S, Kaufmann M, Scherr M, Drexler HG, MacLeod RAF. Activation of HLXB9 by juxtaposition with MYB via formation of t(6;7)(q23;q36) in an AML-M4 cell line (GDM-1). *Genes Chromosomes Cancer*. 2005;42(2):170-178.
21. Thompson N, Gésina E, Scheinert P, Bucher P, Grapin-Botton A. RNA profiling and chromatin immunoprecipitation-sequencing reveal that PTF1a stabilizes pancreas progenitor identity via the control of MNX1/HLXB9 and a network of other transcription factors. *Mol Cell Biol*. 2012;32(6):1189-1199.
22. Rao SSP, Huntley MH, Durand NC, et al. A 3D map of the human genome at kilobase resolution reveals principles of chromatin looping. *Cell*. 2014;159(7):1665-1680.
23. Sollier E, Heilmann J, Gerhauser C, Scherer M, Plass C, Lutsik P. Figeno: multi-region genomic figures with long-read support. *Bioinformatics*. 2024;40(6).
24. Steinek C, Ortiz MG, Stumberger G, et al. Generation of densely labeled oligonucleotides for the detection of small genomic elements. *bioRxiv*. Preprint posted online 15 March 2024. https://doi.org/10.1101/2024.03.15.583980
25. Brandstetter K, Zülske T, Ragoczy T, et al. Differences in nanoscale organization of regulatory active and inactive human chromatin. *Biophys J*. 2022;121(6):977-990.
26. Bintu B, Mateo LJ, Su J-H, et al. Super-resolution chromatin tracing reveals domains and cooperative interactions in single cells. *Science*. 2018;362(6413):eaau1783.
27. Wurm CA, Neumann D, Schmidt R, Egner A, Jakobs S. Sample preparation for STED microscopy. *Methods Mol Biol*. 2010;591:185-199.

28. Robinson JT, Thorvaldsdóttir H, Winckler W, et al. Integrative genomics viewer. *Nat Biotechnol*. 2011;29(1):24-26.
29. Bolouri H, Farrar JE, Triche T Jr, et al. The molecular landscape of pediatric acute myeloid leukemia reveals recurrent structural alterations and age-specific mutational interactions. *Nat Med*. 2018;24(1):103-112.
30. Schwaller J. Novel insights into the role of aberrantly expressed MNX1 (HLXB9) in infant acute myeloid leukemia. *Haematologica*. 2019;104(1):1-3.
31. Balgobind BV, Van den Heuvel-Eibrink MM, De Menezes RX, et al. Evaluation of gene expression signatures predictive of cytogenetic and molecular subtypes of pediatric acute myeloid leukemia. *Haematologica*. 2011;96(2):221-230.
32. Tosi S, Hughes J, Scherer SW, et al. Heterogeneity of the 7q36 breakpoints in the t(7;12) involving ETV6 in infant leukemia. *Genes Chromosomes Cancer*. 2003;38(2):191-200.
33. Waraky A, Östlund A, Nilsson T, et al. Aberrant MNX1 expression associated with t(7;12)(q36;p13) pediatric acute myeloid leukemia induces the disease through altering histone methylation. *Haematologica*. 2024;109(3):725-739.
34. Dalla-Favera R, Lombardi L, Pelicci PG, Lanfrancone L, Cesarman E, Neri A. Mechanism of activation and biological role of the c-myc oncogene in B-cell lymphomagenesis. *Ann N Y Acad Sci*. 1987;511:207-218.
35. Duan H, Xiang H, Ma L, Boxer LM. Functional long-range interactions of the IgH 3' enhancers with the bcl-2 promoter region in t(14;18) lymphoma cells. *Oncogene*. 2008;27(53):6720-6728.
36. Ryan RJH, Drier Y, Whitton H, et al. Detection of enhancer-associated rearrangements reveals mechanisms of oncogene dysregulation in B-cell lymphoma. *Cancer Discov*. 2015;5(10):1058-1071.
37. Northcott PA, Lee C, Zichner T, et al. Enhancer hijacking activates GFI1 family oncogenes in medulloblastoma. *Nature*. 2014;511(7510):428-434.
38. Xu J, Song F, Lyu H, et al. Subtype-specific 3D genome alteration in acute myeloid leukaemia. *Nature*. 2022;611(7935):387-398.
39. Ingenhag D, Reister S, Auer F, et al. The homeobox transcription factor HB9 induces senescence and blocks differentiation in hematopoietic stem and progenitor cells. *Haematologica*. 2019;104(1):35-46.
40. Wildenhain S, Ingenhag D, Ruckert C, et al. Homeobox protein HB9 binds to the prostaglandin E receptor 2 promoter and inhibits intracellular cAMP mobilization in leukemic cells. *J Biol Chem*. 2012;287(48):40703-40712.
41. Kodgule R, Goldman JW, Monovich AC, et al. ETV6 deficiency unlocks ERG-dependent microsatellite enhancers to drive aberrant gene activation in B-lymphoblastic leukemia. *Blood Cancer Discov*. 2023;4(1):34-53.
42. Ragusa D, Dijkhuis L, Pina C, Tosi S. Mechanisms associated with t(7;12) acute myeloid leukaemia: from genetics to potential treatment targets. *Biosci Rep*. 2023;43(1).